

Stochastic gravitational wave background from cosmological neutrino-dominated accretion flows

YUN-FENG WEI¹ AND TONG LIU¹

¹*Department of Astronomy, Xiamen University, Xiamen, Fujian 361005, China*

ABSTRACT

We investigate the stochastic gravitational wave background (SGWB) from neutrino-dominated accretion flows (NDAFs) based on the results of our fallback core-collapse supernova (CCSN) simulations. We find that the predicted SGWB is mainly determined by the typical CCSN initial explosion energy and progenitor metallicity. For the optimistic cases in which the typical initial explosion energy is low, the SGWB from NDAFs without disk outflows might be detected by next-generation space-based interferometers such as Decihertz Interferometer Gravitational wave Observatory (DECIGO) and Big Bang Observer (BBO). In the low-frequency regime $\sim 10^{-3} - 10^{-1}$ Hz, this background is comparable to that expected from standard inflationary models. Therefore, the SGWB from NDAFs may become a foreground for searches of the SGWB generated in the inflationary epoch. Combining the diffuse NDAF neutrino background and SGWB from NDAFs, one may constrain the properties of the CCSNe and NDAFs.

Keywords: Accretion (14); Black holes (162); Core-collapse supernovae (304); Massive stars (732); Gravitational wave astronomy (675)

1. INTRODUCTION

The stochastic gravitational wave background (SGWB) is expected to be created by the superposition of gravitational waves (GWs) from many uncorrelated sources. Such a background could be produced in many processes during cosmological and astrophysical evolutions. A cosmological SGWB may be produced by inflation (e.g., Grishchuk 1975; Starobinskiĭ 1979; Easther & Lim 2006; Smith et al. 2006; Kuroyanagi et al. 2009; Barnaby et al. 2012), cosmic strings (e.g., Caldwell & Allen 1992; Damour & Vilenkin 2000, 2005; Siemens et al. 2007; Ölmez et al. 2010, 2012), alternative cosmologies (e.g., Gasperini & Veneziano 1993; Mandic & Buonanno 2006), and a variety of other phenomena. Astrophysical SGWB could have various possible sources (see Regimbau (2011) for a review), including inspiral and coalescence of compact binaries (e.g., Phinney 1991; Kosenko & Postnov 1998; Regimbau & de Freitas Pacheco 2006; Zhu et al. 2011a; Rosado 2011; Marassi et al. 2011; Wu et al. 2012; Zhu et al. 2013; Evangelista & de Araujo

2015; Evangelista & de Araujo 2015), white dwarf binaries (e.g., Farmer & Phinney 2003), rotating neutron stars (NSs, e.g., Regimbau & de Freitas Pacheco 2001; Ferrari et al. 1999; Houser et al. 1994; Lai & Shapiro 1995; Zhu et al. 2011b; Lasky et al. 2013), core-collapse supernovae (CCSNe, e.g., Ferrari et al. 1999), gamma-ray bursts (GRBs, e.g., Hiramatsu et al. 2005), Population III (Pop III) stars (e.g., Suwa et al. 2007; Marassi et al. 2009), stellar core collapse (e.g., Crocker et al. 2015, 2017), and so on.

The next-generation space GW detectors, such as Decihertz Interferometer Gravitational wave Observatory (DECIGO, Seto et al. 2001) and Big Bang Observer (BBO, Ungarelli et al. 2005), targeting 0.1–1 Hz, might be possible to detect SGWB from both cosmological and astrophysical origins. Notably, these experiments are expected to detect the primordial SGWB that arises in the very early universe during the inflationary epoch (Maggiore 2000). Such SGWB may serve as a powerful tool for studying the extremely early universe. However, astrophysical foreground sources could be a significant problem for searches of the inflationary SGWB. The SGWB from CCSNe (Buonanno et al. 2005) and Population III stars (Suwa et al. 2007; Marassi et al. 2009) are expected to be comparable to or mask the inflationary SGWB in some range of frequencies. Thus, a

good understanding of astrophysical foregrounds around the deci-Hertz band is essential for DECIGO and BBO detecting the inflationary SGWB. In this paper, we focus on the low-frequency GW generated by anisotropic neutrino emission of neutrino-dominated accretion flows (NDAFs) and estimate the SGWB spectrum from NDAFs.

NDAFs around rotating stellar-mass black holes (BHs) are one of the plausible candidates of GRB central engines in massive collapsars and compact object mergers. In the collapsar model (e.g., Woosley 1993; MacFadyen & Woosley 1999) for long-duration GRBs, the core collapse of a massive star can produce a BH hyperaccretion system via the fallback process. For the very high accretion rate, the disk might be in a state of NDAFs. In the inner region of the disk, photons are trapped, and only neutrinos are emitted from the disk surface. These neutrinos annihilate in the space out of the disk and then form the primordial fireball to power a GRB. The properties of NDAFs have been widely studied in recent decades (see e.g., Popham et al. 1999; Narayan et al. 2001; Kohri & Mineshige 2002; Lee et al. 2005; Gu et al. 2006; Chen & Beloborodov 2007; Janiuk et al. 2007; Kawanaka & Mineshige 2007; Liu et al. 2007, 2014; Lei et al. 2009; Xue et al. 2013; Song et al. 2016), and for a review see Liu et al. (2017a). In particular, the GW signals generated by the anisotropic neutrino emission from NDAFs have been investigated by some previous works (e.g., Liu et al. 2017b; Wei & Liu 2020; Song et al. 2020; Wei et al. 2021; Chen et al. 2022; Qi et al. 2022). The neutrino-induced GWs are detectable for ~ 10 Mpc by DECIGO/BBO (Suwa & Murase 2009). Of course, the BZ mechanism (Blandford & Znajek 1977) could coexist even be dominated in the BH hyperaccretion process, but it has no GW radiation.

An earlier estimation of the SGWB produced by NDAFs was given by Suwa & Murase (2009). They adopted some typical GW energy spectra of NDAFs to calculate the SGWB. Meanwhile, they used the GRB formation history to estimate the event rate of NDAFs. The results show that the SGWB from NDAFs is below the detection limit of DECIGO/BBO. However, the effects of progenitor properties and the initial explosion energy on the GW spectrum of NDAF are not included in their work. Besides, the event rate of NDAFs might be underestimated. In the collapsar model, an observable GRB is only triggered when jets launched by the central engine can break out from the envelope and circumstellar medium in the prompt emission phase (Wei & Liu 2022). If the jet is choked in the envelope or the observer is not in the jet’s line of sight, no GRB

would be detected. Therefore, the event rate of GRBs should be much less than that of NDAFs. Of course, the GWs from NDAFs are partly anisotropic. In this work, we estimate the SGWB from NDAFs based on fallback CCSN simulations. In Wei et al. (2021), we revealed how the GW emission of NDAFs depends on the initial explosion energies, masses, and metallicities of the progenitor stars. Here, we aim to improve the estimation of the SGWB from NDAFs by including those dependencies.

In this work, we mainly focus on the SGWB from NDAFs around BHs. Note that NDAFs around NSs may also operate in some GRBs and CCSNe (e.g., Zhang & Dai 2010; Perna et al. 2014). Actually, for the newborn NSs in the center of massive collapsars, their strong magnetic fields ($\gtrsim 10^{15}$ G, see e.g., Song & Liu 2023) will restrain the accretion process and destroy the inner region of the disk. Besides, since the rapidly decreasing fallback accretion rate, NDAFs might only exist for the very initial stage of the NS hyperaccretion process. Therefore, the contribution of NDAFs around NSs to the SGWB is not considered here.

The paper is organized as follows. In Section 2, we describe the setup of our CCSN simulations and discuss the effects of the initial explosion energies and the masses and metallicities of the progenitor stars on the GW emission of NDAFs. In Section 3, we estimate the amplitude of the SGWB from NDAFs. We discuss how the SGWB depends on the initial explosion energy and progenitor metallicity. We also explore the effect of initial mass function (IMF) on the SGWB from NDAFs. The conclusions and discussion are presented in Section 4.

2. MODEL

2.1. CCSN simulations

Here, we briefly review the setup of our CCSN simulations. In this paper, we adopt the presupernova (pre-SN) models with initial mass in the range of $20 - 40 M_{\odot}$ as progenitor models (e.g., Woosley et al. 2002; Woosley & Heger 2007; Heger & Woosley 2010). For those models, the models with zero metallicity ($Z/Z_{\odot} = 0$) and solar metallicity ($Z/Z_{\odot} = 1$) are referenced from Heger & Woosley (2010) and Woosley & Heger (2007), respectively, as well as the ones with metallicity $Z/Z_{\odot} = 0.01$ are provided by Prof. Alexander Heger in private communication, where Z_{\odot} represents the metallicity of the Sun. The stellar collapse and explosion simulations (Liu et al. 2021a; Wei & Liu 2022) are performed in a series of 1D simulations with the Athena++ code (White et al. 2016). We use the piston approach (Woosley & Weaver 1995; Woosley et al. 2002) to carry

out spherically symmetric explosion simulations. For each progenitor star, a piston was initially located at the outer edge of the iron core. When the star collapses, the piston firstly moves inward for 0.45 s and then moves outward with an initial high velocity and decelerates smoothly until coming to rest at 10^9 cm. We follow this approach to determine the initial explosion condition at the inner boundary.

The simulation was divided into two steps to reflect the initial collapse and the subsequent explosion. In the first step, the numerical grid has an inner boundary at 10^9 cm, and a unidirectional outflowing inner boundary condition was used at the inner boundary to mimic the suction effect resulting from the hypothetical piston moving inwards. The outer boundary is set at the surface of the progenitor star. In this step, the grid has 10^4 cells with a logarithmic uniform interval for the radial direction. The simulation is run to 0.45 s, and then the piston turns outwards, corresponding to the outward propagation of the blast.

In the second step, we use the same outflowing inner boundary condition, which is set at 10^9 cm. The outer boundary is set at 10^{16} cm, and the medium outside the star is maintained in a constant state with a pressure and density three orders of magnitude lower than the corresponding ones on the star surface. In this step, the grid has 2,000 logarithmic cells. At the beginning of this step, we map the results of the first step to the new grid for the second step and inject energy into the innermost cell adjacent to the inner boundary to mimic the outward blast passing through the inner boundary. Here, the injected energy is the setting energy, which is assumed to have three values for each case, i.e., 2, 4, and 8 B ($1\text{B} = 10^{51}$ erg). All simulations were run until the remnant growth ceased. For more details of simulations, see Liu et al. (2021a) and Wei & Liu (2022).

For each simulation, we record the evolution of the fallback mass supply rate at the inner boundary. Ignoring the disk outflows, we roughly consider the mass supply rate as the mass accretion rate of the disk. If the mass accretion is high, the hyperaccretion disk would be in the state of NDAFs. Meanwhile, the mass and spin of the BH will violently evolve within tens of seconds. According to the conversion of the energy and angular momentum, the evolution equations of a spinning BH can be expressed as (e.g., Hou et al. 2014; Song et al. 2015),

$$\frac{dM_{\text{BH}}}{dt} = \frac{\dot{M}}{\sqrt{3x_{\text{ms}}}} \left(4 - \frac{3a_*}{\sqrt{x_{\text{ms}}}} \right), \quad (1)$$

and

$$\frac{da_*}{dt} = \frac{2\sqrt{3}\dot{M}}{M_{\text{BH}}} \left(1 - \frac{a_*}{\sqrt{x_{\text{ms}}}} \right)^2, \quad (2)$$

where M_{BH} and \dot{M} are the mass of the BH and the mass accretion rate, respectively, a_* is the dimensionless spin parameter of the BH, and $x_{\text{ms}} = 3 + Z_2 - \sqrt{(3 - Z_1)(3 + Z_1 + 2Z_2)}$ is the dimensionless radius of the marginally stable orbit (Bardeen et al. 1972; Kato et al. 2008), where $Z_1 = 1 + (1 - a_*^2)^{1/3} [(1 + a_*)^{1/3} + (1 - a_*)^{1/3}]$ and $Z_2 = \sqrt{3a_*^2 + Z_1^2}$ for $0 < a_* < 1$.

In this work, the initial spin parameter is set as $a_* = 0.9$, and the starting time is set at the time when the initial BH mass (core mass) reaches $2.3 M_{\odot}$.

2.2. GWs from NDAFs

Neutrino emission of NDAFs is mainly determined by the mass accretion rate and the properties of central BH (Liu et al. 2016; Wei et al. 2019). In the relativistic global solutions of NDAFs (Xue et al. 2013), the detailed neutrino physics, the nuclear statistical equilibrium, and the conditions of the ignition and neutrino trapping are all considered. For the case of the viscosity parameter $\alpha = 0.1$, we can derive the fitting formula for the neutrino luminosity as a function of the BH mass and spin and the mass accretion rate, which is expressed as

$$\log L_{\nu} \text{ (erg s}^{-1}\text{)} = 52.80 - 0.03m_{\text{BH}} + 1.01a_* + 1.08 \log \dot{m}, \quad (3)$$

where $m_{\text{BH}} = M_{\text{BH}}/M_{\odot}$ and $\dot{m} = \dot{M}/M_{\odot} \text{ s}^{-1}$ are the dimensionless BH mass and accretion rate, respectively. It should be noticed that the ignition and trapping accretion rates are roughly ~ 0.001 and $\sim 5 M_{\odot} \text{ s}^{-1}$, respectively, which also be significantly affected by the BH mass and spin and disk viscosity parameter (e.g., Chen & Beloborodov 2007; Zalamea & Beloborodov 2011; Xue et al. 2013; Liu et al. 2017a). But $\sim 0.01 M_{\odot} \text{ s}^{-1}$ can be considered as the minimum accretion rate for detectable neutrino radiation from BH-NDAF systems in the center of massive collapsars (e.g., Liu et al. 2016).

Here, we estimate the GWs from anisotropic neutrino emission, which is firstly proposed by Epstein (1978). We follow the formalism developed by previous works (e.g., Burrows & Hayes 1996; Mueller & Janka 1997; Kotake et al. 2007; Suwa & Murase 2009) to calculate the neutrino-induced GW signals. For a geometrically thin disk model for NDAFs, the local energy flux of GWs can be written as (for details, see Suwa & Murase

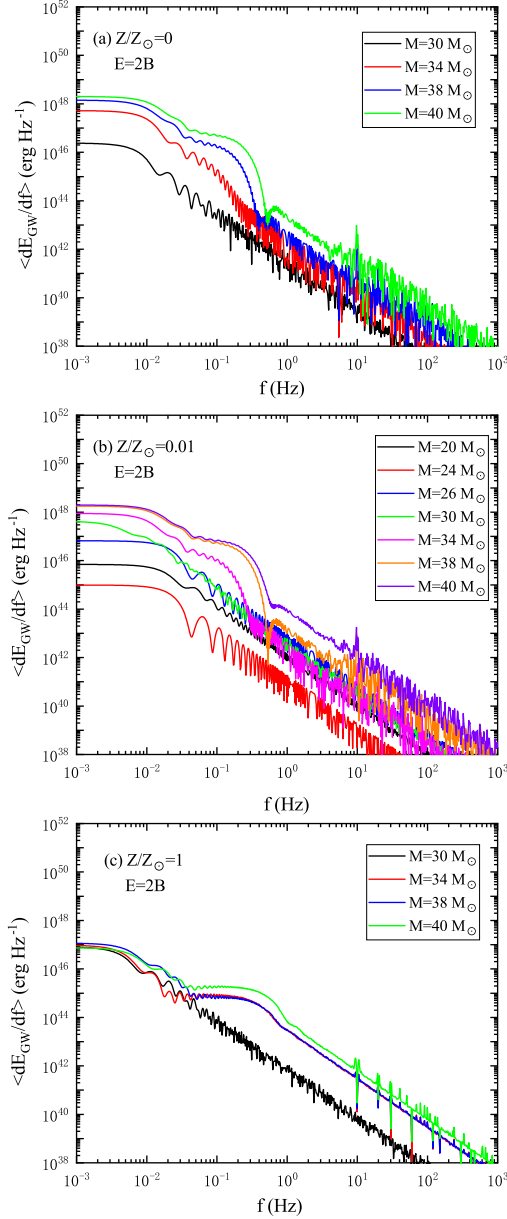


Figure 1. The GW energy spectra of NDAFs with different progenitor masses and metallicities. Panels (a), (b), and (c) correspond to the cases of progenitors with metallicity of $Z/Z_{\odot} = 0, 0.01, \text{ and } 1$, respectively. The initial explosion energy is 2 B.

(2009))

$$\frac{dE_{\text{GW}}}{dA} = \frac{G}{36\pi c^5 D^2} (1 + 2\cos\theta)^2 \tan^4\left(\frac{\theta}{2}\right) \times \int_{-\infty}^{\infty} dt L_{\nu}(t)^2, \quad (4)$$

where $dA = D^2 d\Omega$ is the surface element, D is the distance between the observer and the source, θ is the viewing angle. Here, $\theta = \pi/2$ corresponds to the case that the observer is located in the equatorial plane. Then,

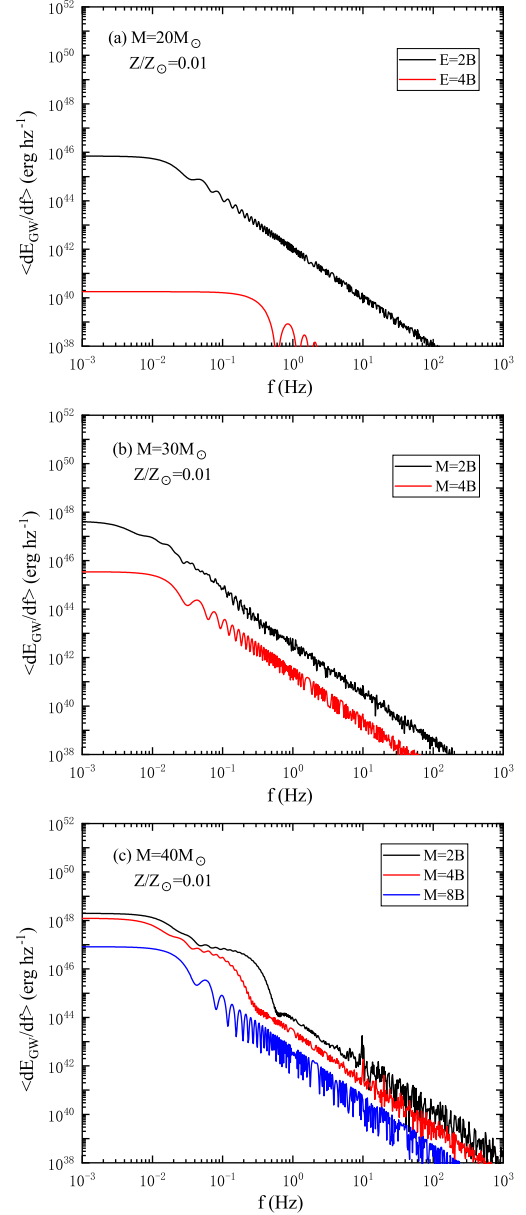


Figure 2. The GW energy spectra of NDAFs with different initial explosion energies. Panels (a), (b), and (c) correspond to the cases of progenitors with mass of 20, 30, and 40 M_{\odot} , respectively. The metallicity is set as $Z/Z_{\odot} = 0.01$.

integrating over a sphere surrounding the source, one can calculate the total energy E_{GW} . For $\theta = \pi/2$, the E_{GW} is calculated as

$$E_{\text{GW}} = \frac{\beta G}{9c^5} \int_{-\infty}^{\infty} dt L_{\nu}(t)^2, \quad (5)$$

where $\beta \sim 0.47039$. In order to calculate GW spectrum, one can write $L_{\nu}(t)$ in terms of the inverse Fourier transform as

$$L_{\nu}(t) = \int_{-\infty}^{+\infty} \tilde{L}_{\nu}(f) e^{-2\pi i f t} df; \quad (6)$$

Table 1. M_{\min} for different metallicities and initial explosion energies.

Metallicity (Z/Z_{\odot})	Initial Explosion Energy (B)	M_{\min} (M_{\odot})
0	2	30
0.01	2	20
1	2	30
0.01	4	20
0.01	8	40

then, the GW energy spectrum can be deduced as

$$\frac{dE_{\text{GW}}(f)}{df} = \frac{2\beta G}{9c^5} \left| \tilde{L}_{\nu}(f) \right|^2. \quad (7)$$

In this work, we assume the orientation of disks is random and calculate the angle average GW energy spectrum per NDAF as

$$\left\langle \frac{dE_{\text{GW}}(f)}{df} \right\rangle = \sum_i \frac{\int_{\Delta\theta_i} d\theta}{\int_0^{\pi/2} d\theta} \frac{dE_{\text{GW},i}(f)}{df} \quad (8)$$

where $\Delta\theta_i$ is the angle range of angle bin i , and $\frac{dE_{\text{GW},i}(f)}{df}$ is the observed GW energy spectrum at the corresponding viewing angle. In the subsequent calculations, we all adopt angle-averaged GW energy spectra.

The effects of the progenitor mass and metallicity on the GW energy spectrum of NDAFs are displayed in Figure 1. Panels (a), (b), and (c) correspond to the cases of progenitors with metallicity of $Z/Z_{\odot} = 0, 0.01,$ and $1,$ respectively. The initial explosion energy is 2 B. In Panels (a) and (c), we only show GW energy spectra of NDAFs from progenitors with a mass greater than $30 M_{\odot}$. In our simulations, for progenitors with metallicities of $Z/Z_{\odot} = 0$ and $1,$ the final remnant of progenitors with a mass less than $30M_{\odot}$ are NSs rather than BHs. The GW amplitude is mainly determined by the neutrino luminosity, which is related to the mass accretion rate. Most of the fallback and neutrino emission come from the core of the star. Therefore, the GW emission of the NDAF is determined by the compactness of the pre-SN star core. Some previous works (e.g., O'Connor & Ott 2011; Sukhbold & Woosley 2014) studied the dependences of progenitor masses and metallicities on the structural characteristics of pre-SN stars and found a non-monotonic behavior for compactness as a function of progenitor mass and metallicity. As a result, for the same initial explosion energy, the GW emission of NDAFs is not strictly dependent on progenitor mass and metallicity. Besides, previous stellar evolutionary studies (Sukhbold & Woosley 2014) found that the core compactness parameters of solar metallicity stars are

commonly smaller than those of low metallicity stars. Thus, solar metallicity is unfavorable for neutrino emission and GW emission of NDAFs. Moreover, although the accretion rate is still large for massive progenitors, the central BH mass is more massive which will influence the neutrino luminosity of NDAFs (Liu et al. 2021b).

Figure 2 shows the effects of the initial explosion energy on the GW energy spectra of NDAFs. The metallicity is set to $Z/Z_{\odot} = 0.01.$ The black, red, and blue curves correspond to the initial explosion energies of 2, 4, and 8 B, respectively. For different progenitor stars, the amplitudes of the spectral lines increase with decreasing initial explosion energy because the weaker explosion energy corresponds to a more powerful fallback and neutrino emission. In Figures 2(a) and 2(b), the case of 8 B is not shown because the final remnants of these progenitors are both NSs.

3. SGWB FROM NDAFS

A prediction of the SGWB requires a good understanding of the average GW energy spectrum and the event rate of NDAFs. The properties of progenitors and the initial explosion energy would determine whether the fallback process produces NDAFs and GW emission of NDAFs. Here, we investigate the effects of metallicities and initial explosion energies of progenitors on SGWB from NDAFs.

3.1. Cosmic NDAF history

The progenitor stars of CCSNe have relatively short lifetimes ($\lesssim 10^8$ years) compared to cosmic timescales (Kennicutt 1998). Thus, the rate of NDAFs can be calculated using the star formation rate and IMF. The cosmic NDAF rate at a redshift of z is calculated as

$$R_{\text{NDAF}}(z) = R_{\text{SFR}}(z) \frac{\int_{M_{\min}}^{M_{\max}} \Psi(M) dM}{\int_{0.1}^{125} M \Psi(M) dM}, \quad (9)$$

where $R_{\text{SFR}}(z)$ is the cosmic star formation rate in units of $\text{Mpc}^{-3} \text{yr}^{-1}$, which can be deduced from observations (e.g., Hopkins & Beacom 2006; Reddy et al. 2008; Rujopakarn et al. 2010). Here, we adopt the continuous broken power law description by Yüksel et al. (2008),

$$R_{\text{SFR}}(z) = \dot{\rho}_0 \left[(1+z)^{\alpha} + \left(\frac{1+z}{C}\right)^{\beta} + \left(\frac{1+z}{D}\right)^{\gamma} \right]^{1/\eta} \quad (10)$$

where $\alpha = 3.4,$ $\beta = -0.3,$ $\gamma = -2,$ $\eta = -10,$ $C \simeq 5100,$ $D \simeq 14,$ and $\dot{\rho}_0 = 0.014 \text{ Mpc}^{-3} \text{yr}^{-1}.$ Here, we adopt a Salpeter IMF (Salpeter 1955) with $\Psi(M) \propto M^{\zeta}$ with $\zeta = -2.35$ in the mass range of $0.1 - 125 M_{\odot},$ but explore a liberal range from -2.15 to -2.45 (Bastian et al. 2010) in our final calculations. M_{\max} and M_{\min} are the maximum and minimum masses of progenitors that produce

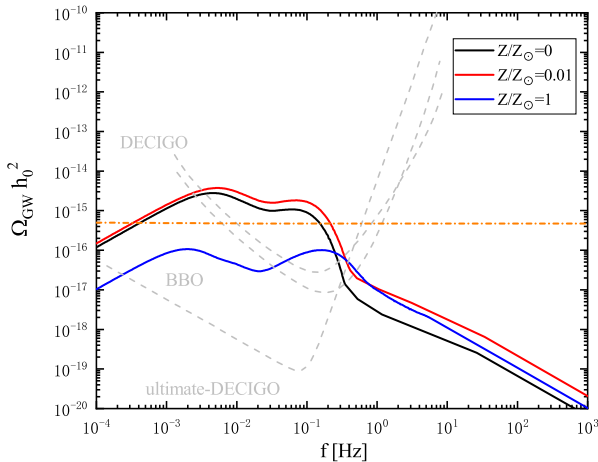


Figure 3. The energy density parameter of SGWB for different metallicities with the initial explosion energy $E = 2 M_\odot$. The horizontal orange dashed line shows the SGWB generated during slow-roll inflation assuming $T/S = 0.3$ for the ratio of the tensorial and scalar contributions to the cosmic microwave background radiation anisotropy and no running of the tensorial power-law index (Turner 1997). The gray dashed lines represent the sensitivity curves of the indicated detectors.

BH-NDAF systems, respectively. Due to the influence of the metallicity of the progenitor and initial explosion energy on the fallback process of CCSNe, not all massive stars can produce NDAFs. Especially, M_{min} depends on the metallicity of progenitor and initial explosion energy (Liu et al. 2021a). According to the results of our simulations, we gave M_{min} for different metallicity and initial explosion energy, and the results are listed in Table 1. Of course, we also checked that the fallback accretion rates of these progenitors are suitable for NDAFs until they decrease lower than the ignition accretion rates. The SGWB prediction depends weakly on the M_{max} and we set $M_{\text{max}} \sim 50 M_\odot$, which is the approximately upper limit of the progenitor mass for NDAFs because the newborn BH mass is too larger to effectively ignite NDAFs (Liu et al. 2021b).

3.2. IMF-weighted average GW energy spectra

The average GW energy spectrum for a population of progenitors is computed by weighting each progenitor by

$$\frac{dE(f)}{df} = \sum_i \frac{\int_{\Delta M_i} \Psi(M) dM}{\int_{M_{\text{min}}}^{M_{\text{max}}} \Psi(M) dM} \langle \frac{dE_{\text{GW}}(f)}{df} \rangle_i, \quad (11)$$

where $\Psi(M)$ is once again the IMF, ΔM_i is the mass range of mass bin i , and $\langle \frac{dE_{\text{GW}}(f)}{df} \rangle_i$ is the angle-averaged GW energy spectrum of the NDAF with progenitor mass of M_i .

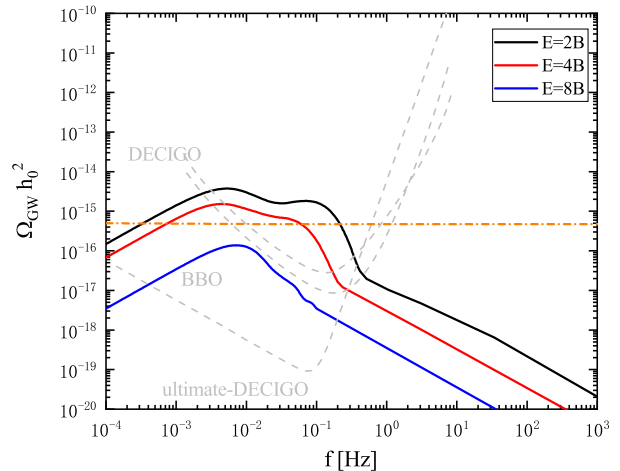


Figure 4. The energy density parameter of SGWB for different initial explosion energies with metallicity $Z/Z_\odot = 0.01$.

3.3. Estimations of SGWB

It is usually to characterize the SGWB by the energy density parameter (Allen & Romano 1999), i.e.,

$$\Omega_{\text{GW}}(f) = \frac{1}{\rho_c} \frac{d\rho_{\text{GW}}}{d \ln f}, \quad (12)$$

where ρ_{GW} is the gravitational energy density and $\rho_c = 3H_0^2/8\pi G$ is the critical energy density needed to close the universe. Then, following Phinney (2001), the sum of the energy densities radiated by a large number of independent NDAFs at each redshift is given as

$$\Omega_{\text{GW}}(f) = \frac{1}{\rho_c c^2} \times \int_0^\infty dz \frac{R_{\text{NDAF}}(z)}{1+z} \left| \frac{dt}{dz} \right| f(z) \frac{dE(f_z)}{df}, \quad (13)$$

where $f_z \equiv f(1+z)$ and $|dt/dz| = [H_0(1+z)\sqrt{\Omega_\Lambda + \Omega_m(1+z)^3}]^{-1}$. Here, we ignore the anisotropy of GWs from NDAFs and adopt the cosmological parameters $\Omega_m = 0.3$, $\Omega_\Lambda = 0.7$, and $H_0 = 100h_0 \text{ km s}^{-1} \text{ Mpc}^{-1}$ with $h_0 = 0.72$.

Figure 3 shows the effect of the metallicity of the progenitor on the spectrum of SGWB from NDAFs. The initial explosion energy of all progenitors is set as $2 M_\odot$. The black, red, and blue curves correspond to $Z/Z_\odot = 0, 0.01, \text{ and } 1$, respectively. The gray dashed lines represent the sensitivity curves of DECIGO (Yagi & Seto 2017; Isoyama et al. 2018; Kawamura et al. 2021), BBO (Crowder & Cornish 2005; Corbin & Cornish 2006), and the ultimate-DECIGO (Seto et al. 2001). Solar metallicity is not beneficial for the detection of the SGWB from NDAFs. This is because the solar metallicity is unfavorable for neutrino emission and GW emission of NDAFs. Moreover, if the solar metallicity is uni-

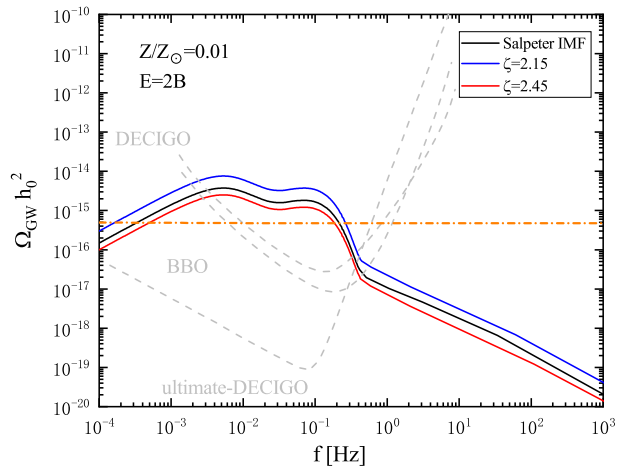


Figure 5. The energy density parameter of SGWB for different IMF. The initial explosion energies is 2 B and metallicity is $Z/Z_\odot = 0.01$.

versal, the event rate of NDAFs would decrease. The horizontal orange dashed line shows the SGWB generated in the inflationary epoch. In low-frequency region ($\sim 10^{-3} - 10^{-1}$ Hz), our estimate for the SGWB from NDAFs can be comparable to the most optimistic SGWB from slow-roll inflation.

In Figure 4, we display the effects of the initial explosion energy on the spectrum of SGWB. We assume all progenitors have the same metallicity, $Z/Z_\odot = 0.01$. The black, red, and blue curves correspond to the initial explosion energy of 2, 4, and 8 B, respectively. The weaker explosion energy corresponds to a more powerful fallback, which enhances the GW emission and the event rate of NDAFs. As a result, the initial explosion energy will significantly affect the detection of the SGWB from NDAFs.

In Figure 5, we explore the effect of IMF on the spectrum of SGWB from NDAFs. The black curve corresponds to the Salpeter IMF with $\zeta = -2.35$. The red and blue curves correspond to $\zeta = -2.15$ and $\zeta = -2.45$, respectively. A shallower IMF (i.e., $\zeta = -2.15$) is beneficial for the detection of SGWB from NDAFs. The SGWB differs by almost a factor of 3 between the case of $\zeta = -2.15$ and the case of $\zeta = -2.45$. As shown in Figure 1, for the same progenitor metallicity and initial explosion energy, relatively higher mass stars correspond to the higher accretion rate, then the more powerful GW emission of NDAFs until the effects of the central BH mass dominate the ignition of NDAFs. Shallower IMFs have more high-mass stars which contribute to the SGWB.

4. CONCLUSIONS AND DISCUSSION

In this paper, we estimate the SGWB produced by NDAFs based on fallback CCSN simulations. The effects of progenitor properties and initial explosion energies on SGWB from NDAFs are studied. These factors can affect the GW energy spectra and event rates of NDAFs. The GW emission of NDAFs is determined by the fallback process in CCSNe. Lower initial explosion energy is beneficial for producing a more powerful fallback, resulting in stronger neutrino emission and GW emission of NDAFs. Moreover, low initial explosion energy may enhance the event rates of NDAFs. Therefore, if low initial explosion energy is universal CCSNe, even for failed CCSNe, the SGWB from NDAFs may be detected by interferometers such as DECIGO and BBO. The influence of metallicity on SGWB from NDAFs is not monotonic because the compactness of the pre-SN star core is not strictly dependent on metallicity. However, solar metallicity is not beneficial for the detection of SGWB. Another uncertainty in our models is the IMF. A shallower IMF would increase the amplitude of SGWB from NDAFs. Therefore, the SGWB could be a valuable tool to investigate the IMF.

In NDAF models, we adopt $\alpha = 0.1$ as a typical viscosity parameter. Actually, a disk with low α is denser and has a higher neutrino luminosity (e.g., Popham et al. 1999; Liu et al. 2007; Chen & Beloborodov 2007; Liu et al. 2017a). Thus, the GW emission of NDAFs with low α might be more powerful. Besides, in our calculations, we do not consider the disk outflows, which plays an important role in critical accretion systems (e.g. Liu et al. 2008, 2014; Gu 2015). The neutrino luminosity of NDAFs with strong disk outflows would be at least one order of magnitude lower than that of NDAFs without outflows (Liu et al. 2021b). As a result, powerful disk outflow will decrease the GW emission of NDAFs. If powerful disk outflows are universal in NDAFs, the amplitude of SGWB from NDAFs would decrease.

In summary, the uncertainties of the SGWB from NDAFs are large. The detection of the corresponding neutrino background will lead to an improved prediction of the SGWB from NDAFs. In Wei et al. (2024), we investigated the diffuse NDAF neutrino background (DNNB) in detail. Metallicity and initial explosion energy have similar effects on both DNNB and SGWB from NDAFs. For the optimistic cases where the typical initial explosion energy is low, the DNNB might be detected by the upcoming larger neutrino detectors such as Hyper-Kamiokande, Jiangmen Underground Neutrino Observatory (JUNO), and Deep Underground Neutrino Experiment (DUNE). The detection of DNNB would help constrain the average neutrino emission and event

rate of NDAFs. By combining the DNNB and SGWB, we would better understand CCSNe and NDAFs.

It is noted that the SGWB from NDAFs might mask the SGWB generated in the inflationary epoch at low frequency. Besides, the SGWB from cosmological CCSNe and Pop III stars are expected to mask the inflationary GWs in some range of frequencies. These astrophysical foreground sources could be a significant problem for searches of the inflationary SGWB. It is necessary to disentangle these foreground sources from the inflationary SGWB in future detection.

ACKNOWLEDGMENTS

We thank Prof. Alexander Heger for providing us pre-SN data. We also thank Xing-Jiang Zhu for helpful discussion. This work was supported by the National Key R&D Program of China (Grant No. 2023YFA1607902), the National Natural Science Foundation of China (Grant Nos. 12173031, 12221003, and 12303049), the Postdoctoral Fellowship Program of China Postdoctoral Science Foundation (Grant No. GZC20231424), and the science research grants from the China Manned Space Project.

REFERENCES

- Allen, B. & Romano, J. D. 1999, *PhRvD*, 59, 102001.
doi:10.1103/PhysRevD.59.102001
- Bardeen, J. M., Press, W. H., & Teukolsky, S. A. 1972, *ApJ*, 178, 347. doi:10.1086/151796
- Barnaby, N., Pajer, E., & Peloso, M. 2012, *PhRvD*, 85, 023525. doi:10.1103/PhysRevD.85.023525
- Bastian, N., Covey, K. R., & Meyer, M. R. 2010, *ARA&A*, 48, 339. doi:10.1146/annurev-astro-082708-101642
- Blandford, R. D. & Znajek, R. L. 1977, *MNRAS*, 179, 433. doi:10.1093/mnras/179.3.433
- Buonanno, A., Sigl, G., Raffelt, G. G., et al. 2005, *PhRvD*, 72, 084001. doi:10.1103/PhysRevD.72.084001
- Burrows, A. & Hayes, J. 1996, *PhRvL*, 76, 352. doi:10.1103/PhysRevLett.76.352
- Caldwell, R. R. & Allen, B. 1992, *PhRvD*, 45, 3447. doi:10.1103/PhysRevD.45.3447
- Chen, B.-G., Liu, T., Qi, Y.-Q., et al. 2022, *ApJ*, 941, 156. doi:10.3847/1538-4357/aca406
- Chen, W.-X. & Beloborodov, A. M. 2007, *ApJ*, 657, 383. doi:10.1086/508923
- Corbin, V. & Cornish, N. J. 2006, *Classical and Quantum Gravity*, 23, 2435. doi:10.1088/0264-9381/23/7/014
- Crocker, K., Mandic, V., Regimbau, T., et al. 2015, *PhRvD*, 92, 063005. doi:10.1103/PhysRevD.92.063005
- Crocker, K., Prestegard, T., Mandic, V., et al. 2017, *PhRvD*, 95, 063015. doi:10.1103/PhysRevD.95.063015
- Crowder, J. & Cornish, N. J. 2005, *PhRvD*, 72, 083005. doi:10.1103/PhysRevD.72.083005
- Damour, T. & Vilenkin, A. 2000, *PhRvL*, 85, 3761. doi:10.1103/PhysRevLett.85.3761
- Damour, T. & Vilenkin, A. 2005, *PhRvD*, 71, 063510. doi:10.1103/PhysRevD.71.063510
- Easther, R. & Lim, E. A. 2006, *JCAP*, 2006, 010. doi:10.1088/1475-7516/2006/04/010
- Epstein, R. 1978, *ApJ*, 223, 1037. doi:10.1086/156337
- Evangelista, E. F. D. & de Araujo, J. C. N. 2015, *MNRAS*, 449, 2700. doi:10.1093/mnras/stv473
- Farmer, A. J. & Phinney, E. S. 2003, *MNRAS*, 346, 1197. doi:10.1111/j.1365-2966.2003.07176.x
- Ferrari, V., Matarrese, S., & Schneider, R. 1999, *MNRAS*, 303, 247. doi:10.1046/j.1365-8711.1999.02194.x
- Gasperini, M. & Veneziano, G. 1993, *Astroparticle Physics*, 1, 317. doi:10.1016/0927-6505(93)90017-8
- Grishchuk, L. P. 1975, *Soviet Journal of Experimental and Theoretical Physics*, 40, 409
- Gu, W.-M. 2015, *ApJ*, 799, 71. doi:10.1088/0004-637X/799/1/71
- Gu, W.-M., Liu, T., & Lu, J.-F. 2006, *ApJL*, 643, L87. doi:10.1086/505140
- Harry, G. M., Fritschel, P., Shaddock, D. A., et al. 2006, *Classical and Quantum Gravity*, 23, 4887. doi:10.1088/0264-9381/23/15/008
- Harry, G. M., Fritschel, P., Shaddock, D. A., et al. 2006, *Classical and Quantum Gravity*, 23, C01. doi:10.1088/0264-9381/23/24/C01
- Heger, A. & Woosley, S. E. 2010, *ApJ*, 724, 341. doi:10.1088/0004-637X/724/1/341
- Hiramatsu, T., Kotake, K., Kudoh, H., et al. 2005, *MNRAS*, 364, 1063. doi:10.1111/j.1365-2966.2005.09643.x
- Hopkins, A. M. & Beacom, J. F. 2006, *ApJ*, 651, 142. doi:10.1086/506610
- Hou, S.-J., Liu, T., Gu, W.-M., et al. 2014, *ApJL*, 781, L19. doi:10.1088/2041-8205/781/1/L19
- Houser, J. L., Centrella, J. M., & Smith, S. C. 1994, *PhRvL*, 72, 1314. doi:10.1103/PhysRevLett.72.1314
- Isoyama, S., Nakano, H., & Nakamura, T. 2018, *Progress of Theoretical and Experimental Physics*, 2018, 073E01. doi:10.1093/ptep/pty078
- Janiuk, A., Yuan, Y., Perna, R., et al. 2007, *ApJ*, 664, 1011. doi:10.1086/518761

- Kato, S., Fukue, J., & Mineshige, S. 2008, *Black-Hole Accretion Disks: Towards a New Paradigm*, Kyoto University Press (Kyoto, Japan).
- Kawamura, S., Ando, M., Seto, N., et al. 2021, *Progress of Theoretical and Experimental Physics*, 2021, 05A105. doi:10.1093/ptep/ptab019
- Kawanaka, N. & Mineshige, S. 2007, *ApJ*, 662, 1156. doi:10.1086/517985
- Kennicutt, R. C. 1998, *ARA&A*, 36, 189. doi:10.1146/annurev.astro.36.1.189
- Kohri, K. & Mineshige, S. 2002, *ApJ*, 577, 311. doi:10.1086/342166
- Kosenko, D. I. & Postnov, K. A. 1998, *A&A*, 336, 786. doi:10.48550/arXiv.astro-ph/9801032
- Kotake, K., Ohnishi, N., & Yamada, S. 2007, *ApJ*, 655, 406. doi:10.1086/509320
- Kowalska-Leszczynska, I., Regimbau, T., Bulik, T., et al. 2015, *A&A*, 574, A58. doi:10.1051/0004-6361/201424417
- Kudoh, H., Taruya, A., Hiramatsu, T., et al. 2006, *PhRvD*, 73, 064006. doi:10.1103/PhysRevD.73.064006
- Kuroyanagi, S., Chiba, T., & Sugiyama, N. 2009, *PhRvD*, 79, 103501. doi:10.1103/PhysRevD.79.103501
- Lai, D. & Shapiro, S. L. 1995, *ApJ*, 442, 259. doi:10.1086/175438
- Lasky, P. D., Bennett, M. F., & Melatos, A. 2013, *PhRvD*, 87, 063004. doi:10.1103/PhysRevD.87.063004
- Lee, W. H., Ramirez-Ruiz, E., & Page, D. 2005, *ApJ*, 632, 421. doi:10.1086/432373
- Lei, W. H., Wang, D. X., Zhang, L., et al. 2009, *ApJ*, 700, 1970. doi:10.1088/0004-637X/700/2/1970
- Liu, T., Gu, W.-M., Xue, L., et al. 2007, *ApJ*, 661, 1025. doi:10.1086/513689
- Liu, T., Gu, W.-M., Xue, L., et al. 2008, *ApJ*, 676, 545. doi:10.1086/527670
- Liu, T., Gu, W.-M., & Zhang, B. 2017a, *NewAR*, 79, 1. doi:10.1016/j.newar.2017.07.001
- Liu, T., Lin, C.-Y., Song, C.-Y., et al. 2017b, *ApJ*, 850, 30. doi:10.3847/1538-4357/aa92c4
- Liu, T., Qi, Y.-Q., Cai, Z.-Y., et al. 2021b, *ApJ*, 920, 5. doi:10.3847/1538-4357/ac1428
- Liu, T., Wei, Y.-F., Xue, L., et al. 2021a, *ApJ*, 908, 106. doi:10.3847/1538-4357/abd24e
- Liu, T., Yu, X.-F., Gu, W.-M., et al. 2014, *ApJ*, 791, 69. doi:10.1088/0004-637X/791/1/69
- Liu, T., Zhang, B., Li, Y., et al. 2016, *PhRvD*, 93, 123004. doi:10.1103/PhysRevD.93.123004
- MacFadyen, A. I. & Woosley, S. E. 1999, *ApJ*, 524, 262. doi:10.1086/307790
- Maggiore, M. 2000, *PhR*, 331, 283. doi:10.1016/S0370-1573(99)00102-7
- Mandic, V. & Buonanno, A. 2006, *PhRvD*, 73, 063008. doi:10.1103/PhysRevD.73.063008
- Marassi, S., Schneider, R., Corvino, G., et al. 2011, *PhRvD*, 84, 124037. doi:10.1103/PhysRevD.84.124037
- Marassi, S., Schneider, R., & Ferrari, V. 2009, *MNRAS*, 398, 293. doi:10.1111/j.1365-2966.2009.15120.x
- Mueller, E. & Janka, H.-T. 1997, *A&A*, 317, 140
- Narayan, R., Piran, T., & Kumar, P. 2001, *ApJ*, 557, 949. doi:10.1086/322267
- O'Connor, E. & Ott, C. D. 2011, *ApJ*, 730, 70. doi:10.1088/0004-637X/730/2/70
- Owen, B. J., Lindblom, L., Cutler, C., et al. 1998, *PhRvD*, 58, 084020. doi:10.1103/PhysRevD.58.084020
- Ölmez, S., Mandic, V., & Siemens, X. 2010, *PhRvD*, 81, 104028. doi:10.1103/PhysRevD.81.104028
- Ölmez, S., Mandic, V., & Siemens, X. 2012, *JCAP*, 2012, 009. doi:10.1088/1475-7516/2012/07/009
- Perna, R., Duffell, P., Cantiello, M., et al. 2014, *ApJ*, 781, 119. doi:10.1088/0004-637X/781/2/119
- Phinney, E. S. 1991, *ApJL*, 380, L17. doi:10.1086/186163
- Phinney, E. S. 2001, *astro-ph/0108028*. doi:10.48550/arXiv.astro-ph/0108028
- Popham, R., Woosley, S. E., & Fryer, C. 1999, *ApJ*, 518, 356. doi:10.1086/307259
- Qi, Y.-Q., Liu, T., Huang, B.-Q., et al. 2022, *ApJ*, 925, 43. doi:10.3847/1538-4357/ac3757
- Reddy, N. A., Steidel, C. C., Pettini, M., et al. 2008, *ApJS*, 175, 48. doi:10.1086/521105
- Regimbau, T. 2011, *Research in Astronomy and Astrophysics*, 11, 369. doi:10.1088/1674-4527/11/4/001
- Regimbau, T. & de Freitas Pacheco, J. A. 2001, *A&A*, 376, 381. doi:10.1051/0004-6361:20011005
- Regimbau, T. & de Freitas Pacheco, J. A. 2006, *ApJ*, 642, 455. doi:10.1086/500190
- Rosado, P. A. 2011, *PhRvD*, 84, 084004. doi:10.1103/PhysRevD.84.084004
- Rujopakarn, W., Eisenstein, D. J., Rieke, G. H., et al. 2010, *ApJ*, 718, 1171. doi:10.1088/0004-637X/718/2/1171
- Salpeter, E. E. 1955, *ApJ*, 121, 161. doi:10.1086/145971
- Seto, N. 2008, *ApJL*, 683, L95. doi:10.1086/591847
- Seto, N., Kawamura, S., & Nakamura, T. 2001, *PhRvL*, 87, 221103. doi:10.1103/PhysRevLett.87.221103
- Siemens, X., Mandic, V., & Creighton, J. 2007, *PhRvL*, 98, 111101. doi:10.1103/PhysRevLett.98.111101
- Smith, T. L., Kamionkowski, M., & Cooray, A. 2006, *PhRvD*, 73, 023504. doi:10.1103/PhysRevD.73.023504
- Song, C.-Y. & Liu, T. 2023, *ApJ*, 952, 156. doi:10.3847/1538-4357/acd6ee
- Song, C.-Y., Liu, T., Gu, W.-M., et al. 2015, *ApJ*, 815, 54. doi:10.1088/0004-637X/815/1/54

- Song, C.-Y., Liu, T., Gu, W.-M., et al. 2016, MNRAS, 458, 1921. doi:10.1093/mnras/stw427
- Song, C.-Y., Liu, T., & Wei, Y.-F. 2020, MNRAS, 494, 3962. doi:10.1093/mnras/staa932
- Starobinskiĭ, A. A. 1979, Soviet Journal of Experimental and Theoretical Physics Letters, 30, 682
- Sukhbold, T. & Woosley, S. E. 2014, ApJ, 783, 10. doi:10.1088/0004-637X/783/1/10
- Suwa, Y. & Murase, K. 2009, PhRvD, 80, 123008. doi:10.1103/PhysRevD.80.123008
- Suwa, Y., Takiwaki, T., Kotake, K., et al. 2007, ApJL, 665, L43. doi:10.1086/521078
- Turner, M. S. 1997, PhRvD, 55, R435. doi:10.1103/PhysRevD.55.R435
- Ungarelli, C., Corasaniti, P., Mercer, R. A., et al. 2005, Classical and Quantum Gravity, 22, S955. doi:10.1088/0264-9381/22/18/S09
- Wei, Y.-F. & Liu, T. 2020, ApJ, 889, 73. doi:10.3847/1538-4357/ab6325
- Wei, Y.-F. & Liu, T. 2022, ApJ, 936, 182. doi:10.3847/1538-4357/ac8bd1
- Wei, Y.-F., Liu, T., & Song, C.-Y. 2019, ApJ, 878, 142. doi:10.3847/1538-4357/ab2187
- Wei, Y.-F., Liu, T., & Song, C.-Y. 2024, ApJ, 966, 101. doi:10.3847/1538-4357/ad3824
- Wei, Y.-F., Liu, T., & Xue, L. 2021, MNRAS, 507, 431. doi:10.1093/mnras/stab2153
- White, C. J., Stone, J. M., & Gammie, C. F. 2016, ApJS, 225, 22. doi:10.3847/0067-0049/225/2/22
- Woosley, S. E. 1993, ApJ, 405, 273. doi:10.1086/172359
- Woosley, S. E. & Heger, A. 2007, PhR, 442, 269. doi:10.1016/j.physrep.2007.02.009
- Woosley, S. E., Heger, A., & Weaver, T. A. 2002, Reviews of Modern Physics, 74, 1015. doi:10.1103/RevModPhys.74.1015
- Woosley, S. E. & Weaver, T. A. 1995, ApJS, 101, 181. doi:10.1086/192237
- Wu, C., Mandic, V., & Regimbau, T. 2012, PhRvD, 85, 104024. doi:10.1103/PhysRevD.85.104024
- Xue, L., Liu, T., Gu, W.-M., et al. 2013, ApJS, 207, 23. doi:10.1088/0067-0049/207/2/23
- Yagi, K. & Seto, N. 2017, PhRvD, 95, 109901. doi:10.1103/PhysRevD.95.109901
- Yüksel, H., Kistler, M. D., Beacom, J. F., et al. 2008, ApJL, 683, L5. doi:10.1086/591449
- Zalamea I., & Beloborodov A. M., 2011, MNRAS, 410, 2302. doi:10.1111/j.1365-2966.2010.17600.x
- Zhang, D. & Dai, Z. G. 2010, ApJ, 718, 841. doi:10.1088/0004-637X/718/2/841
- Zhu, X.-J., Fan, X.-L., & Zhu, Z.-H. 2011b, ApJ, 729, 59. doi:10.1088/0004-637X/729/1/59
- Zhu, X.-J., Howell, E., Regimbau, T., et al. 2011a, ApJ, 739, 86. doi:10.1088/0004-637X/739/2/86
- Zhu, X.-J., Howell, E. J., Blair, D. G., et al. 2013, MNRAS, 431, 882. doi:10.1093/mnras/stt207